Chemical Engineering Faculty Publications   Department of Chemical Engineering

2004

Mechanistic and Bifurcation Analysis of Anode Potential Oscillations in Pemfcs with CO in Anode Feed

J. X. Zhang

Joseph D. Fehribach
Worcester Polytechnic Institute, bach@wpi.edu

Ravindra Datta
Worcester Polytechnic Institute, rdatta@wpi.edu

Mechanistic and Bifurcation Analysis of Anode Potential Oscillations in PEMFCs with CO in Anode Feed

Jingxin Zhang,[a,*] **Joseph D. Fehribach,**[b,**] **and Ravindra Datta**[a,**,z]

[a]*Fuel Cell Center, Department of Chemical Engineering, Worcester Polytechnic Institute, Worcester, Massachusetts 01609, USA*
[b]*Department of Mathematical Sciences, Worcester Polytechnic Institute, Worcester, Massachusetts 01609, USA*

A detailed mathematical analysis is performed to understand the anode potential oscillations observed experimentally in a proton exchange membrane fuel cell (PEMFC) with H_2/CO feed (Ref. 9). Temperature and anode flow rate are found to be key bifurcation parameters. The time dependence of all the key surface species must be accounted for in order for the model to predict the oscillatory behavior, while the time dependence of CO concentration in the anode chamber need not necessarily be considered. The bifurcation diagram of CO electro-oxidation rate constant agrees very well with the effect of temperature on the oscillation pattern. The oscillator model is classified as a hidden negative differential resistance oscillator based on the dynamical response of the anodic current and surface species to a dynamic potential scan. A linear stability analysis indicates that the bifurcation experienced is a supercritical Hopf bifurcation.
© 2004 The Electrochemical Society. [DOI: 10.1149/1.1688795] All rights reserved.

There is great interest in the development of cost effective and high-performance proton exchange membrane fuel cells (PEMFCs) for applications in the automotive and consumer electronics industries.[1] A stumbling block in the commercialization of PEMFCs, however, is the storage and distribution of H_2, which is the ideal fuel for a low-temperature, high-power-density fuel cell. As an alternative, reformate gas containing CO_2 and traces of CO in addition to H_2 obtained from methanol or gasoline is also being investigated.[2] Furthermore, direct use of methanol,[3] propanol,[4] or formic acid[5] as the anode feed is also being attempted for PEMFCs in order to reduce system complexity and increase overall efficiency.

PEMFCs may be operated in a constant current, constant voltage, or constant resistance mode. It is theoretically conceivable that spontaneous periodic behavior may appear in this electrochemical reaction system due to the interplay of such factors as chemical and electrochemical reactions, mass transfer, current, and electrode potential.[6,7] The presence of CO, which is either a feed impurity (in reformate fuel) or a reaction intermediate (in direct fuel cells), increases the tendency of such a self-organized instability to appear.[8] Our earlier experiments indicated that periodic potential oscillations exist when the fuel cell is operating with H_2 containing CO and with PtRu as anode catalyst at a constant current density.[9] These spontaneous oscillations were observed over a practical operating temperature range (room temperature to about 80°C) and current densities.

Although potential oscillations in PEMFCs have only recently been reported, the observation of spontaneous potential or current oscillations in other electrochemical systems is not uncommon.[6,10-12] Nonlinear dynamics in electrochemical reactions has been reviewed by Hudson and Tsotsis.[10] Various examples of oscillatory behavior in electrochemical reaction systems can be found in this exhaustive review. Koper described the importance of negative differential resistance to the instability of an electrochemical system.[11] It was also shown rigorously that the frequency response method is very powerful in evaluating the stability of electrochemical systems. Examples of how the frequency response theory can be applied to such systems can be found in Ref. 11. An experimental strategy was proposed by Strasser *et al.*[13] in an attempt to classify the known electrochemical oscillators based on mechanisms. Krischer recently reviewed the current understanding of basic principles governing temporal and spatial behavior in electrochemical systems exhibiting dynamic instability.[6] It is acknowledged that conditions far from thermodynamic equilibrium and appropriate feedback should be present for the occurrence of self-organized phenomena. The dynamic instability is linked to the interplay of the electrode kinetics, transport processes occurring in the electrolyte, and the external electrical circuit. Consequently, the differential equations governing the temporal evolution of these systems are derived from charge as well as mass balance.

Undoubtedly, the potential oscillations observed in PEMFCs serve as another interesting and important case for the study of electrochemical oscillators. Thus, analysis of such oscillatory phenomenon is essential for its understanding and classification in the family of electrochemical oscillators. Moreover, although the phenomenological characterizations and modeling interpretation are abundant in the literature,[8,14-17] a mathematical bifurcation analysis is still warranted. In a mechanistic analysis study by Strasser *et al.*,[18] two simplified generic models describing electrochemical reaction systems have been discussed qualitatively in terms of the possible sign pattern of the Jacobian and nature of the eigenvalues. As far as we know, no quantitative demonstration of bifurcation analysis for a PEMFC system has been presented so far. This paper thus presents the first quantitative linear stability analysis on a realistic model describing the dynamic behavior of a PEMFC anode reaction system.

A detailed numerical analysis of a mechanistic model is given here in terms of the existing theory of electrochemical oscillators. The essential components for describing the experimentally observed oscillation behavior are identified. The model is further classified as a hidden negative differential resistance (HNDR) oscillator based upon the dynamic response of the system. Finally, one-parameter bifurcation diagrams are discussed, followed by a local linear stability analysis (details in the Appendix). Thus, a Hopf bifurcation is quantitatively demonstrated in the fuel-cell system.

Experimental

The experimental details can be found in our previous work.[19] A brief description is given here. Gas diffusion electrodes loaded with 20 wt % Pt/C or PtRu/C, at a metal loading of 0.4 and 0.35 mg/cm^2, respectively, were purchased from E-TEK. PtRu/C was used as anode catalyst, while the cathode catalyst was Pt/C. Nafion 115 proton-exchange membranes (PEMs; Du Pont, Fayetteville, PA) were used after treatment. The membrane electrode assembly (MEA) was prepared by hot-pressing in a model C Carver hot press at 130°C and under a pressure of 4000 lbs for about 2 min. The MEA was then incorporated in a 5 cm^2 single cell from Electro-Chem, Inc. (Woburn, MA), and tested in a test station with temperature, pressure, humidity, and flow rate control. The anode feed is H_2/108 ppm CO and oxygen is used as cathode feed. The fuel cell

* Electrochemical Society Student Member.
** Electrochemical Society Active Member.
z E-mail: rdatta@wpi.edu

Table I. Model parameters used in simulation.

Model parameters

K_{CO}	2×10^{-7} atm[a]	$\vec{k}_{OH}$	8×10^{-4} A cm^{-2b}
K_H	0.5 atm[a]	$\overleftarrow{k}_{OH}$	2760 A cm^{-2c}
α_H	0.5	x_{CO}^0	108×10^{-6}
α_{CO}	0.5	T	315 K
α_{OH}	0.5	C_{dl}	0.45 F^d
$\vec{k}_{H,ox}$	4.0 A cm^{-2a}	γ	100^e
$\vec{k}_{H_2,ad}$	402 A cm^{-2} atm^{-1af}	C_t^*	2.2×10^{-9} mol/cm^{2b}
$\vec{k}_{CO,ad}$	150 A cm^{-2} atm^{-1af}	A	5 cm^2
$\vec{k}_{CO,ox}$	5.5×10^{-4} A cm^{-2b}	P_{H_2}	2.958 atm
i	0.3 A/cm^2	v_0	48.1 sccm
V_A	2.63×10^{-7} m^3		

[a] Ref. 31.
[b] Fitted parameters.
[c] Ref. 8.
[d] Ref. 37.
[e] Estimated by the specific surface area of 20 wt % E-TEK PtRu/C catalyst and an electrochemical efficiency (utilization) of the anode catalyst of about 30%.
[f] These two values have been increased by a factor of 10 from the original value in order to match the simulated oscillation frequency with the experimental results.
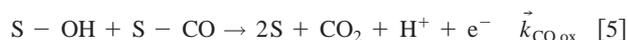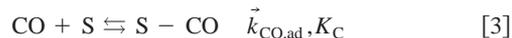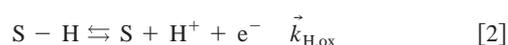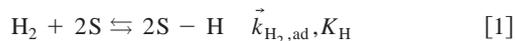
voltage was recorded using an HP 6060B dc electronic load, interfaced with a PC using LabVIEW software (National Instruments, Austin, TX) at a data sampling rate of 77 ms.

In order to monitor the CO concentration in the fuel cell anode outlet gas, the exit gas stream after the back pressure regulator first passes through a stainless steel filter (model 85, Parker Hannifin, Tewksbury, MA) to eliminate any particulates and water droplets. The gas stream then passes through a membrane gas dryer (MD series, Perma Pure, Inc., Toms River, NJ), which further lowers the dew point of the gas stream to below 2°C before admission to the gas analyzer. A model 200 IR gas analyzer (California Analytical Instruments, Orange, CA) was used after calibration to monitor the exit CO concentration. The FP-AI-100 analog input module/FP-1000 network module (National Instruments, Austin, TX) is used to collect data from the gas analyzer with LabVIEW software.

Anode Dynamic Model

The anode kinetic model developed in our previous work[9] is provided here; more details may be found in Ref. 9. The symbols are listed separately. All rates (and rate constants) in the model have been expressed as equivalent current densities (A/cm^2) based on the geometric area of the electrode (Table I).

Surface kinetics.—The model assumes uniform surface sites, represented by S. It is assumed that alloying between Pt and Ru only alters the energetics and kinetics of the surface reactions

$$H_2 + 2S \leftrightarrows 2S - H \quad \vec{k}_{H_2,ad}, K_H \quad [1]$$

$$S - H \leftrightarrows S + H^+ + e^- \quad \vec{k}_{H,ox} \quad [2]$$

$$CO + S \leftrightarrows S - CO \quad \vec{k}_{CO,ad}, K_C \quad [3]$$

$$H_2O + S \leftrightarrows S - OH + H^+ + e^- \quad \vec{k}_{OH}, \overleftarrow{k}_{OH} \quad [4]$$

$$S - OH + S - CO \rightarrow 2S + CO_2 + H^+ + e^- \quad \vec{k}_{CO,ox} \quad [5]$$

The net adsorption rate for H_2 is

$$r_{H_2,ad} = \vec{k}_{H_2,ad} p_{H_2} \theta_0^2 - \overleftarrow{k}_{H_2,ad} K_H \theta_H^2 \quad [6]$$

where θ_0 is from the total site balance

$$\theta_0 = 1 - \theta_{CO} - \theta_H - \theta_{OH} \quad [7]$$

The rate for hydrogen electro-oxidation is

$$r_H = 2\vec{k}_{H,ox}\theta_H \sinh\left(\frac{\alpha_H F \eta_A}{RT}\right) \quad [8]$$

The net rate of CO adsorption is

$$r_{CO,ad} = \vec{k}_{CO,ad} x_{CO} p_{H_2} \theta_0 - \overleftarrow{k}_{CO,ad} K_C \theta_{CO} \quad [9]$$

The water dissociative adsorption rate is

$$r_{OH} = \vec{k}_{OH}\theta_0 \exp\left(\frac{\alpha_{OH}F\eta_A}{RT}\right) - \overleftarrow{k}_{OH}\theta_{OH} \exp\left(\frac{-(1-\alpha_{OH})F\eta_A}{RT}\right) \quad [10]$$

The CO oxidation rate is

$$r_{CO} = \vec{k}_{CO,ox}\theta_{CO}\theta_{OH} \exp\left(\frac{\alpha_{CO}F\eta_A}{RT}\right) \quad [11]$$

Mass and charge conservation.—With these rate expressions we can write the following unsteady-state site balance for the time evolution of the surface coverage of CO, H, and OH

$$(F\gamma C_t^*)\frac{d\theta_{CO}}{dt} = r_{CO,ad} - r_{CO} \quad [12]$$

$$(F\gamma C_t^*)\frac{d\theta_H}{dt} = r_{H_2,ad} - r_H \quad [13]$$

$$(F\gamma C_t^*)\frac{d\theta_{OH}}{dt} = r_{OH} - r_{CO} \quad [14]$$

The following equations govern the time variation of the CO concentration in the anode chamber considered as well-mixed

$$\frac{p_{H_2}V_A}{RT}\frac{dx_{CO}}{dt} = \frac{P_0 v_0}{RT_0}x_{CO}^0 - \frac{P_0 v}{RT_0}x_{CO} - \frac{A}{F}r_{CO,ad} \quad [15]$$

Similarly, balance for H_2 in the anode chamber provides

$$\frac{P_0 v}{RT_0} = \frac{P_0 v_0}{RT_0} - \frac{A}{2F}r_{H_2,ad} \quad [16]$$

Considering capacitive and faradaic currents and using the equation of charge conservation, an equation for the time evolution of the electrode potential is obtained. The total current is the sum of the faradaic current and the capacitive current (double-layer charging and discharging current)

$$C_{dl}\frac{d\eta_A}{dt} = A(i - r_H - r_{CO} - r_{OH}) \quad [17]$$

The resulting system of coupled ordinary differential equations (ODEs; Eq. 12-14,15,17) were solved with Berkeley-Madonna software (Kagi Shareware, Berkeley, CA) using a fourth-order Runge-Kutta routine. This model predicts that periodic potential oscillations exist under our experimental conditions and also provides reasonable prediction of both the oscillation periods and magnitude. The computation results shown in the following section are obtained using parameters given in Ref. 9 unless otherwise noted.

Results and Discussion

Temperature as an experimental bifurcation parameter.—Electrochemical systems, under certain conditions, lose stability upon the change of certain control parameters. Applied potential, applied current, and bulk concentration of reactants are often reported to be such parameters.[7,20,21] However, literature reports on temperature as a bifurcation parameter are rare.[22] During our study of anode potential oscillations in PEMFCs with PtRu anode catalyst,
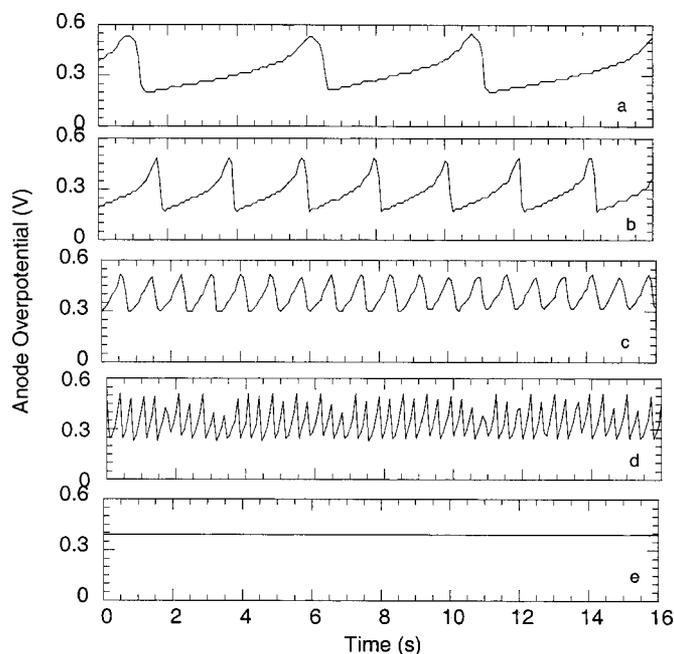
Figure 1. Anode potential patterns (periodic oscillations and stable steady state) in PEMFC at different temperatures and a constant current density. The fuel cell temperature, current density, and anode inlet flow rate are as follows: (a) 32°C, 100 mA/cm², 24.5 sccm; (b) 42°C, 300 mA/cm², 36.4 sccm; (c) 55°C, 300 mA/cm², 48.1 sccm; (d) 70°C, 700 mA/cm², 95.6 sccm; and (e) 80°C, 700 mA/cm², 83.7 sccm. Anode feed H_2/108 ppm CO in all cases. Oscillation patterns are not affected appreciably by the current density and anode inlet flow rate (Ref. 9).

we found that fuel cell temperature is a very sensitive bifurcation parameter. The anode overpotential patterns at five different fuel cell temperatures are shown in Fig. 1. It is seen that for fuel cell temperatures below 70°C, sustained potential oscillations exist under the specified experimental conditions. However, the oscillations disappear at a fuel cell temperature of 80°C and a stable steady state is obtained. Clearly temperature is acting as a bifurcation parameter, upon change of which the system behavior changes. However, temperature effect has rarely been investigated in oscillatory electrochemical systems in the previous literature,[22] possibly because of the use of liquid electrolytes.

Another feature worth mentioning is the change of oscillation period and magnitude with temperature. The oscillation period becomes longer as the temperature reduces from the bifurcation point (somewhere between 70 and 80°C). Moreover, the magnitude of oscillation increases as temperature decreases. These characteristics are very typical for a Hopf bifurcation.

Electrode properties essential for description of nonlinear behavior.—There are two characteristic properties of fuel cell electrodes which are important for the successful description of the dynamic behavior of the anode reaction system. The first one is the anode capacitance, which directly affects the magnitude of the charging and discharging current. As shown in a recent study by Kim *et al.*,[23] the total specific capacitance of a porous carbon electrode is determined primarily by the real surface area of the electrode. It has been determined that for carbon power with Brunauer-Emmett-Teller (BET) surface area of 2408 m²/g, the specific capacitance is 217 F/g.[23] The electrode used in this work is an E-TEK standard double-sided electrode. The carbon power used is Vulcan XC-72 R carbon black with an average particle size of 30 nm and a specific surface area of 254 m²/g.[24] If it is assumed that the capacitance of the carbon power is proportional to the surface area, then the porous carbon in this work can be estimated to have a specific capacitance of 22.9 F/g.
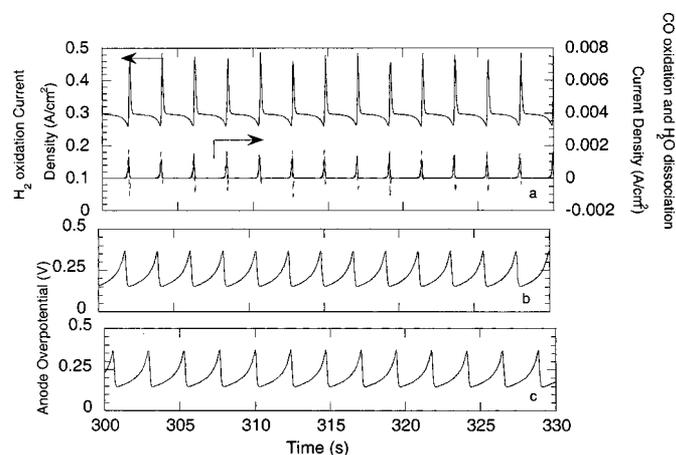

Figure 2. Comparison of the current-providing reactions: (a) Magnitude of H_2 oxidation current, CO oxidation current, and H_2O dissociation current. For right *y* axis, (——) CO oxidation current and (— — —) H_2O dissociation current. (b) Oscillation pattern calculated with all three current-providing reactions. (c) Oscillation pattern calculated with H_2 oxidation current only.

The carbon loading in the diffusion layer[24] is about 4 mg/cm², and the catalyst loading is 0.35 mg/cm². The metal loading (PtRu) in the supported catalyst is 20 wt %. Then the total carbon loading in the anode is about 27 mg (20 mg in the diffusion layer and 7 mg in the catalyst layer). Thus, the total capacitance of the porous electrode in the PEMFC anode in this study is estimated to be 0.62 F. This value agrees reasonably well with the value used previously in the simulation (0.45 F).[9]

The second electrode property of importance in discussing instability is the roughness factor of the electrode, which is used to characterize the real catalyst surface area available per geometric electrode surface area. The reaction rates are directly related to catalytic sites available in the porous electrode. The roughness factor depends on the catalyst loading, the metal particle size (dispersion), and ionomer and poly(tetrafluoroethylene) (PTFE) loading in the electrode.[25] Such dependence is because the electrochemically active catalyst site should be accessible by reactant gas, protons, and electrons simultaneously. The roughness factor in this study was not independently measured but estimated from the literature result. It is reported by Adjemian *et al.*[26] that an average roughness factor of 135 cm²/cm² was found for an E-TEK Pt/C electrode with a Pt loading of 0.4 mg/cm² and an Nafion loading of 0.6 mg/cm². The electrode used in this study is also an E-TEK standard electrode, with the metal particle size and ionomer loading being the same. Thus, the roughness factor of the electrode in this study can be estimated based on actual metal loading. The result obtained (118 cm²/cm²) agrees well with the value used in the simulation (100 cm²/cm²).[9]

Current carrier and essential variables.—An individual electrochemical reaction step within a mechanism of multiple reactions can be considered the "current carrier" of the mechanism if it provides the bulk portion of the total faradaic current at all times. The three contributions of the faradaic current in this anode model, *i.e.*, H_2 electro-oxidation current, CO electro-oxidation current, and H_2O dissociatively adsorption current, are shown in Fig. 2a. It is evident that the contribution from CO electro-oxidation and water dissociation is rather small as compared to that from H_2 oxidation, the difference being at least two orders of magnitude. Thus, the hydrogen electro-oxidation is the major current carrier. When the two minor current contributions are neglected in the overall charge conservation equation (Eq. 17), the model, as expected, can still reproduce the oscillation pattern without appreciable change in the oscillatory behavior (Fig. 2c).
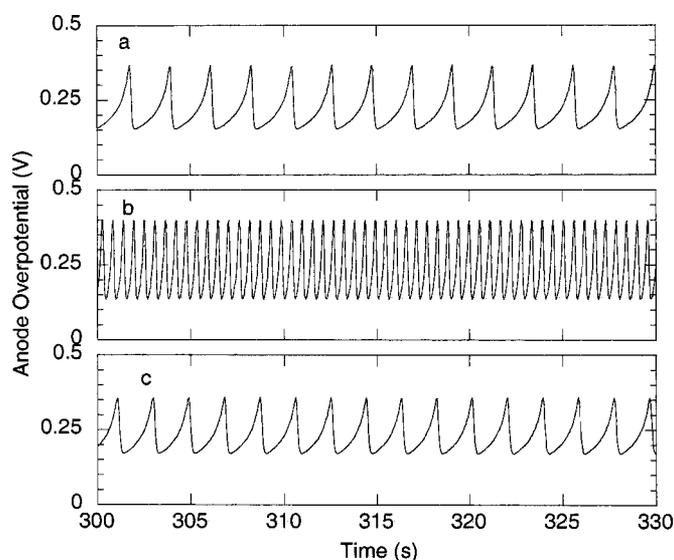
Figure 3. Simulation of oscillation pattern with and without anode CO concentration as a time-dependent variable: (a) CO concentration as a time-dependent variable in the model, (b) with a constant anode CO concentration $x_{co} = 108$ ppm, and (c) with a constant anode CO concentration $x_{co} = 12$ ppm.

Figure 4. Calculated CV of fuel cell anode at a scan rate of 20 mV/s.

It is found computationally that the three surface species (CO, H, OH) are all essential variables, *i.e.*, the time dependence of all these is indispensable for the overall reaction dynamics. No oscillations are obtained when any one of the three surface coverages is set to a constant value. However, the time dependence of anode CO concentration (x_{CO}) is found to be nonessential for the model to predict oscillations. Figure 3 shows the simulated oscillation pattern with the complete model (Fig. 3a) or with constant values of x_{CO} (Fig. 3b and c). Consequently, when the five ODEs are reduced to four, the model still displays oscillatory behavior. However, it is found that the actual value of the constant anode CO concentration has a large effect on the shape of the oscillation pattern. Thus, when the feed CO concentration (108 ppm) is used as the anode chamber CO concentration, the model predicts an oscillation with a much shorter period than that observed experimentally. However, reasonable agreement between experiment and simulation (Fig. 3c) is realized when the assumed constant anode chamber CO concentration is around the CO concentration predicted by the CO mass balance equation. If the assumed CO concentration (x_{CO}) is less than about 8 ppm, no oscillation is predicted by the model. Therefore, although the CO concentration in the anode chamber need not necessarily be time-dependent for the system to demonstrate oscillatory behavior, the steady-state material balance of CO in the anode chamber (Eq. 15 with $dx_{CO}/dt = 0$) is absolutely necessary for the model to reflect the real anode CO concentration as measured experimentally with the CO analyzer,[19] and to reproduce the experimental potential oscillation pattern.

In order to check if the anode CO concentration in an operating fuel cell is oscillating simultaneously with anode overpotential, an on-line CO gas analyzer was used to monitor the anode exit gas steam. We were, however, unable to observe any CO concentration oscillations in the fuel cell anode outlet stream. However, a constant CO concentration of 10 ppm is observed for an inlet CO of 100 ppm, which is in good agreement with the model prediction of a CO concentration between 11 and 13 ppm.

Apart from the possibility that the anode CO concentration does not oscillate in reality, another reason for not observing CO concentration oscillation in our experiment is that the oscillation has a period of only 0.3-5 s, while the response time of the analyzer is on the order of a second at designed flow rate (>500 sccm, while the flow rate used in this study is well below 100 sccm). Thus, the
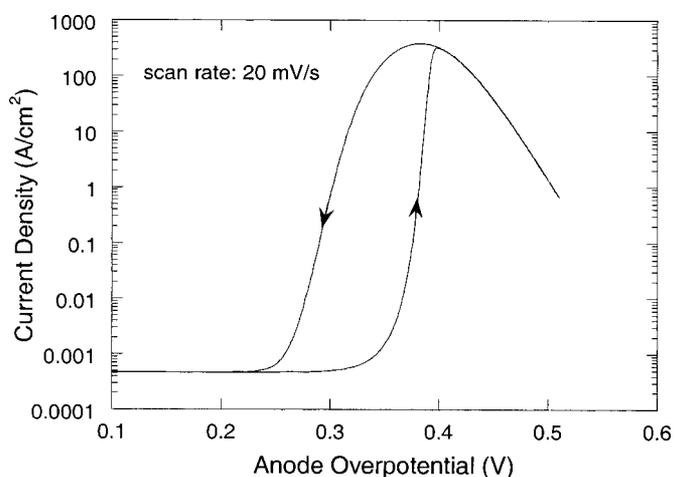
response time of the analyzer is of the same order as the oscillation periods. In addition, the anode outlet gas has to pass a filter and a dryer before admission to the IR gas analyzer; thus, the dispersion effects may smear out any concentration variations during the travel of the gas stream between the anode and the analyzer.

Mechanistic classification of the anode potential oscillation.— There are many oscillatory systems in electrochemical processes. A systematic classification of such oscillators is useful in elucidating and simplifying the origin of the oscillatory behavior. The classification has been based on such factors as the operating conditions, the reaction chemistry, and most recently, on the mechanistic role of potential and chemical species.[13] In this section, the anode model is used to predict the system behavior in a potential scan, the response of which provides insight on the characterization of the oscillatory phenomenon.[6] The calculated cyclic voltammogram (CV) for a linear rate of 20 mV/s is shown in Fig. 4 and 5b. The hydrogen current is assumed unlimited by hydrogen mass transport in the electrode, because the anode limiting current density is usually very large.[25] Thus, the hydrogen limiting current in the anode is not reflected in the computed CV in Fig. 4 and 5b.

In Fig. 4 the overall anode current in the forward and reverse scan is plotted *vs.* the anode overpotential at a scan rate of 20 mV/s. The overall current density does not increase appreciably until an anode overpotential of about 0.35 V is reached in the anodic scan.
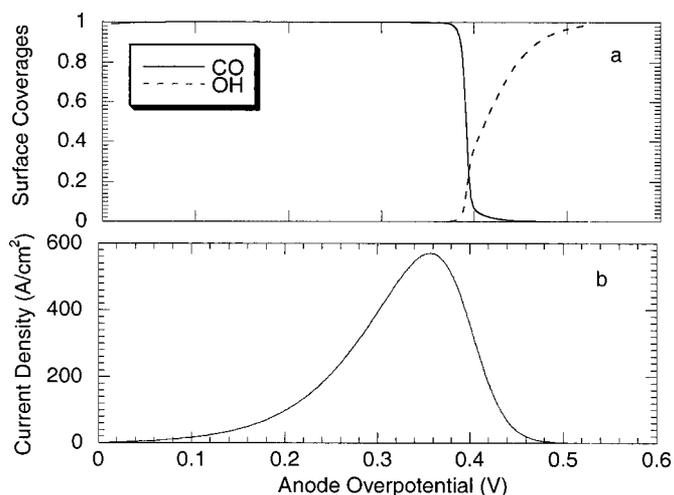

Figure 5. (a) Calculated surface coverage of CO and OH and (b) H_2 oxidation current without the presence of CO in the forward scan at 20 mV/s.

The current increases dramatically after this "ignition potential." However, the current decreases when a peak value is reached at about 0.4 V. In the reverse scan, the overall current density traces the anodic scan in the potential region higher than 0.4 V, but below that, the overall current density does not follow the forward scan. The current begins to drop precipitously only when the anode overpotential is lower by about 50 mV. Thus, a hysterisis is observed in the calculated CV. Hysterisis in a CV during a dynamic potential scan has been observed in the study of H_2/CO electro-oxidation in the liquid electrolyte.[27,28] This dynamic response is especially similar to the experimental CV curve reported by Krischer *et al.*[29] in H_2 electro-oxidation when Cu^{2+} and Cl^- are present in the electrolyte solution (Fig. 13c in Ref. 29).

Hydrogen electro-oxidation is an extremely fast reaction and the initial low current density in Fig. 4 is due to the surface blockage by adsorbed CO. Thus, the corresponding change of surface coverage of both CO and OH in the forward scan is shown in Fig. 5a. It can be seen that the catalyst surface is dominated by CO when the anode overpotential is lower than about 0.38 V. In this potential region hydrogen electro-oxidation can barely proceed on the CO-covered surface. When the anode overpotential is larger than 0.38 V, the surface coverage of CO decreases precipitously, but correspondingly, the surface coverage of OH gradually increases and approaches a saturation value as the anode overpotential further increases. Therefore, the catalyst surface is dominated by OH groups, which leads to the eventual decrease of the overall current density, as shown in Fig. 4. Thus, in this region of the stationary current-potential curve (Fig. 4), a "negative differential resistance" appears, *i.e.*, the total current decreases with the increase of electrode potential. This negative differential resistance is known to be one of several features which are necessary for the existence of electrochemical instability.[7,11] The surface coverage of H is not shown in Fig. 5a; it follows the same trend as the current density in forward scan in Fig. 4.

The negative differential resistance can be seen more clearly in the absence of CO both in the gas phase and on the catalyst surface. The anodic current without CO in the feed is shown in Fig. 5b. The negative polarization slope now appears at a potential of 0.36 V, whereas in the presence of CO (Fig. 4) the current is still increasing at this anode overpotential. Thus, a part of the negative resistance caused by OH nucleation becomes "hidden" via the reactive removal of CO from the catalyst surface with OH. Only after most of the CO has been removed does the effect of the negative faradaic impedance become distinguishable. Moreover, galvanostatic oscillations are found both in our models and in the experiments. All these features are the characteristics of a class of electrochemical oscillator termed as hidden negative differential resistance (HNDR) by Krischer[6] and Strasser *et al.*[13]

A comparison between the PEMFC anode reaction system in this work with examples of HNDR oscillators in the literature further supports this classification. The oscillatory system in this study has the following essential components of an HNDR oscillator: (*i*) a current carrying process (H electro-oxidation, which depends on the anode overpotenital); (*ii*) a process responsible for the occurrence of the negative differential resistance (potential-dependent adsorption and desorption of OH); and (*iii*) a potential-dependent process in which potential has a positive effect on the reaction rate (reactive removal of CO). Another important feature for the HNDR oscillator is the relative time scale of different processes. In this case, the OH adsorption, which is potential dependent, being a very fast process is of prime importance for the occurrence of potential oscillations.

Besides the essential components, the simultaneous presence of a fast positive destabilizing feedback loop and a slow negative stabilizing feedback loop has also been identified in our model, in a manner similar to that of Strasser *et al.*[17] The two feedback loops are depicted in Fig. 6. The positive feedback loop operates as follows: because hydrogen electro-oxidation is the main current-carrying reaction, an increase of the number of free sites results in an increase of H surface coverage, θ_H, which tends to increase the

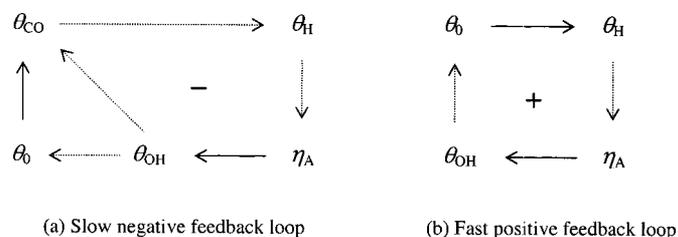(a) Slow negative feedback loop   (b) Fast positive feedback loop

Figure 6. Positive and negative feedback loops in the anode dynamic model. The solid (dashed) arrow indicates a positive (negative) influence. An even number of negative influences lead to a positive effect, and an odd number of negative influences lead to a negative feedback loop.

current (Eq. 8). Because the total current is controlled at a constant value *I*, the system dynamics automatically lowers the anode overpotential, which in turn leads to a reduction of OH (Eq. 10) and release of more free surface sites (Eq. 7). The negative feedback loop is depicted in Fig. 6a. The surface species θ_{CO} participates in this negative feedback loop, which is negatively impacted by θ_{OH} but has a negative effect on θ_H as well. The potential-dependent reduction of surface OH is crucial for the model to reproduce the oscillation phenomenon. If the water dissociation is assumed to be an irreversible step in the model, no oscillations are predicted. Thus, the reverse reaction in Eq. 4 is an essential feedback for the appearance of oscillations. Moreover, the different time scales of CO and OH adsorption are of great importance in the feedback loops of potential oscillations.

The phase angles of different variables are compared in Fig. 7. It can be seen that the variables, though oscillating simultaneously, assume different phase angles. It is seen that the increase of the anode overpotential lags behind the increase of θ_{CO}, while the increase of anode overpotential η induces the increase of θ_{OH}. These two variables are almost in phase, and θ_{OH} follows the variations of η almost without delay. This is in agreement with the fact that the positive feedback loop is a fast one.

As a typical example of an HNDR oscillator, galvanostatic potential oscillation is observed under practical fuel cell operating conditions. It is believed that a potentiostatic current oscillation is also possible for an HNDR oscillator.[6,11] However, current oscillations were not observed when the fuel cell voltage was held constant. One possible reason may be that there is no serial resistance large enough to bring the current and anode potential down to the bifurcation region. It has been reported that current oscillation was observed only after a large serial resistance is introduced.[30] Another possible reason is the self-adjustment of fuel cell electrode potential. In fact, in our fuel cell experiments, it is the potential difference between the anode and cathode that is controlled when the fuel cell voltage is held constant. It was shown by Springer *et al.*[31] that the anode and
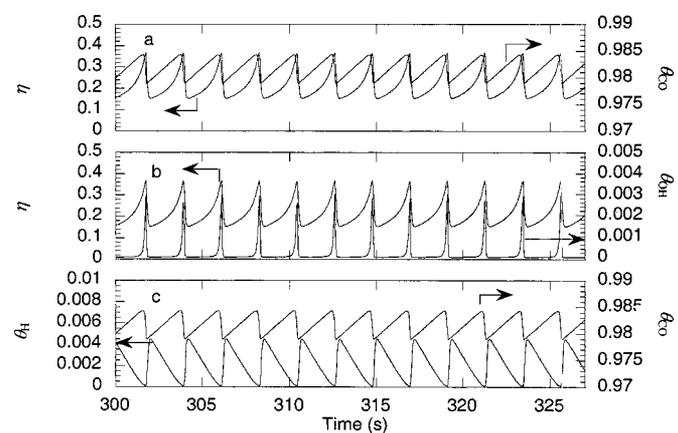

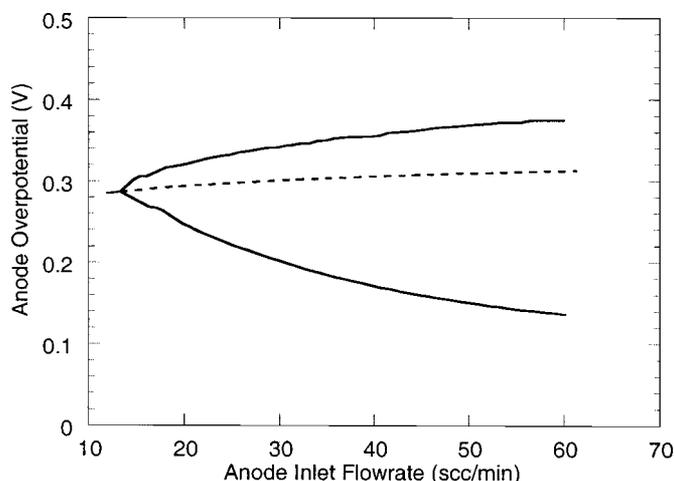**Figure 7.** Comparison of the phase angle of the essential variables.

Figure 8. One-parameter bifurcation diagram for the anode inlet flow rate: (− − −) the unstable steady state, (———) the maximum and minimum overpotential in the oscillations. Temperature 42°C; current density 300 mA/cm^2.

Figure 9. One-parameter bifurcation diagram for the CO electro-oxidation rate constant $\vec{k}_{CO,ox}$. Other conditions as in Fig. 8.

cathode potential has a self-adjustment mechanism in voltage control mode. Thus, the overall potential drop redistributes along anode, membrane, and cathode so as to generate a maximum current, which may be responsible for the disappearance of any current oscillations as well.

One-parameter bifurcation diagrams.—It has been experimentally observed that the potential oscillations set in at certain operation conditions.[9] The fuel cell temperature, current density, and anode flow rate are found to be the key operating parameters affecting the onset of potential oscillations. The one-parameter bifurcation diagrams for these parameters are computed with the anode dynamic model. The bifurcation diagram for the anode inlet flow rate is shown in Fig. 8 for a temperature of 42°C and a current density of 300 mA/cm^2. It can be seen that oscillation starts at a smaller flow rate, which is in agreement with the experimental observations. The oscillation amplitude is predicted to increase with the anode inlet flow rates, which is also observed experimentally.[9] Furthermore, it is predicted that the oscillation period does not change appreciably with the increase of anode inlet flow rate, especially within the flow rate range of the experiment. This is also in agreement with the experimental observations.[9]

As a reflection of the effect of temperature (Fig. 1), the CO electro-oxidation rate constant $\vec{k}_{CO,ox}$ turns out to be a crucial parameter for the shape of the calculated oscillation pattern.[9] The computed one-parameter bifurcation diagram in terms $\vec{k}_{CO,ox}$ is illustrated in Fig. 9. The other model parameters are kept unchanged. The rate constant is related to the fuel cell temperature through the Arrhenius equation. It is shown that for large $\vec{k}_{CO,ox}$ (high temperature), a stable steady-state anode overpotential is observed. As $\vec{k}_{CO,ox}$ decreases (temperature lowers), the stable steady state loses its stability via a supercritical Hopf bifurcation (as discussed in next section). The dashed line in the figure symbolized the unstable steady state, which appears as sustained potential oscillations, with the maximum and minimum overpotential indicated by the upper and lower branch of the solid line. It is shown that the oscillation amplitude is small near the bifurcation point, while the amplitude grows when $\vec{k}_{CO,ox}$ (temperature) is far from the bifurcation point. When $\vec{k}_{CO,ox}$ is small enough (*e.g.*, 5.5×10^{-6}), no oscillatory solution is obtained. Instead, only a steady-state point is found. It should be pointed out that the nonsmoothness in the curve near the bifurcation point in Fig. 8 and 9 is due to the discrete manner in the computation.

It has been shown that potential oscillations do not exist experimentally for PEMFCs with Pt anode under identical experimental
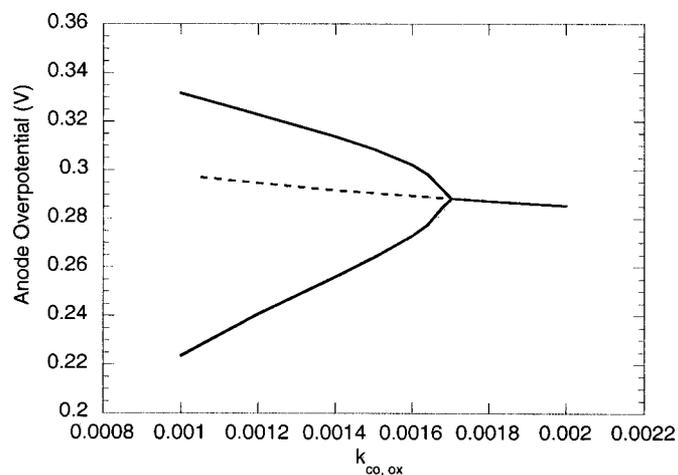
conditions.[9] This observation may be justified mathematically by the model as well. It is computationally found that when the water adsorption rate constant $\vec{k}_{OH}$ is lower than a certain value (*e.g.*, $<1 \times 10^{-5}$ A/cm^2, which corresponds to 4.71×10^{-4} s^{-1}, is similar to the value of 10^{-4} s^{-1} used for $\vec{k}_{OH}$ of Pt in Ref. 8), no oscillation is predicted by the dynamic model. The decrease of water adsorption rate constant may simulate the change of the catalyst from PtRu to Pt. Therefore, the disappearance of oscillations at a smaller water adsorption rate constant in the simulation is reasonably consistent with the experimental fact that oscillation is not observed on the Pt anode.

The bifurcation diagram for the applied current density was also computed. Unfortunately, the predicted bifurcation diagram using the parameter values in our previous work is not able to explain the experimentally observed effect. However, the predictions can be made to match the experimental results by increasing the H$_2$ electro-oxidation rate constant. However, this improvement in the prediction of bifurcation analysis for current density compromises the excellent prediction of the other two bifurcation parameters discussed previously. Thus, it seems that fine tuning of the parameter values used in our simulation is still necessary in order to reproduce all the bifurcation behavior.

In a spatially extended system, self-organization in time is generally accompanied by pattern formation in space.[6,32,33] Although the fuel cell anode chamber and anode surface may be assumed to be homogeneous in this work, a spatial pattern is possible for fuel cells with large electrode area, and in this case space as an additional variable must be taken into account. In fact, the steady-state spatial
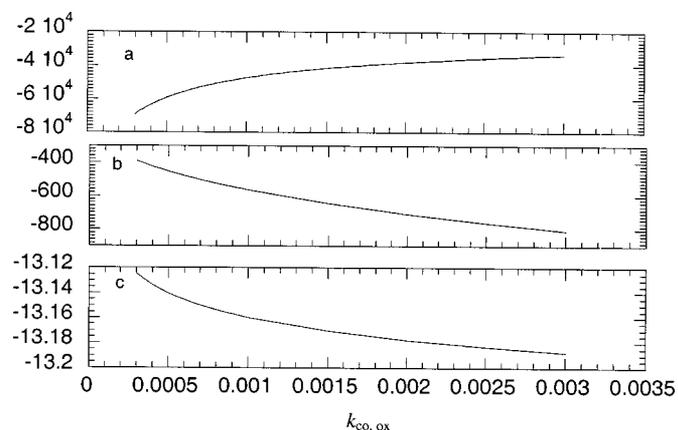

Figure 10. The three real eigenvalues of the dynamic model as a function of the CO electro-oxidation rate constant $\vec{k}_{CO,ox}$.

profile of reactant concentration and current density is now attracting attention.[34,35]

Local linear stability analysis: A Hopf bifurcation.—Spontaneous oscillations in a physicochemical system are generally related to the fact that the stationary state is unstable. The stability of the stationary state may change under the influence of a control parameter and can be studied using bifurcation theory, which is an efficient mathematical tool to analyze a dynamic system. It can predict not only when a certain bifurcation will occur, but also the properties of a bifurcation in a set of differential equations modeling the electrochemical system.[7] For a local bifurcation (*e.g.*, saddle-node bifurcation, Hopf bifurcation), local linear stability analysis can be applied.[7]

The details of the local stability analysis are in the Appendix. The eigenvalues of the system as a function of the bifurcation parameter $\vec{k}_{CO,ox}$ are plotted in Fig. 10a-c and 11. It should be pointed out that plots in Fig. 11 are complex planes, with the x and y axis being the real and imaginary parts of the eigenvalues. It is found that with the decrease of $\vec{k}_{CO,ox}$, the real parts of the two conjugate complex eigenvalues change sign from negative to positive (detailed calculation indicates that the real part passes the imaginary axis at a critical $\vec{k}_{CO,ox}$ value of 0.001679). The equilibrium solution is stable when $\vec{k}_{CO,ox}$ is greater than 0.001679, but the equilibrium solution loses stability as $\vec{k}_{CO,ox}$ decreases below 0.001679. Because the imaginary parts are nonzero and all the other eigenvalues are negative, the Hopf bifurcation theorem[36] allows us to conclude that at least locally (*i.e.*, for parameter values sufficiently close to the critical value), the system undergoes a Hopf bifurcation from which a periodic orbit or limit cycle is born. The periodic orbit emerging from this Hopf bifurcation can be stable or unstable. While it is difficult to prove how much $\vec{k}_{CO,ox}$ can decrease below the critical value before some other bifurcation occurs, numerical (computational) experiments indicate that the oscillatory solution is stable for reasonable values of $\vec{k}_{CO,ox}$ below the critical value.

From the characteristics of both the experiments (Fig. 1) and the simulations (Fig. 14 in Ref. 9), *i.e.*, the oscillations are small amplitude close to the bifurcation point and the amplitude grows and period increases as the bifurcation parameter moves away from the critical value, the bifurcation in terms of fuel cell temperature is a supercritical Hopf bifurcation, which is further proved by the bifurcation diagram and local linear stability analysis. Thus, a coherent picture of Hopf bifurcation in this nonlinear reaction system emerges both experimentally and mathematically.

Conclusions

Temperature is found to be a key bifurcation parameter in anode potential oscillations in PEMFCs. Hydrogen electro-oxidation is the major current-producing reaction, and all the surface species have to be time-dependent in order for the model to predict the oscillatory behavior. However, the CO concentration in the anode chamber need not necessarily be time dependent. The online CO concentration monitoring does not show any oscillation but does confirm the model prediction on the average value of CO concentration. It is possible that any small oscillations in this are smeared out or not measurable by the CO detector.

The oscillation model is classified as an HNDR oscillator based on the response of anodic current and coverage of surface species in a dynamic linear potential scan. Both the bifurcation diagram and a linear stability analysis in terms of the CO electro-oxidation rate constant indicate that the bifurcation experienced during the variation of fuel cell temperature is a supercritical Hopf bifurcation, which leads to stable potential oscillations when the fuel cell is set at constant current density.

As a most promising power source, the unstable steady state (sustained oscillations) in PEMFC operation will undoubtedly attract more attention, both in terms of the manipulation of the system
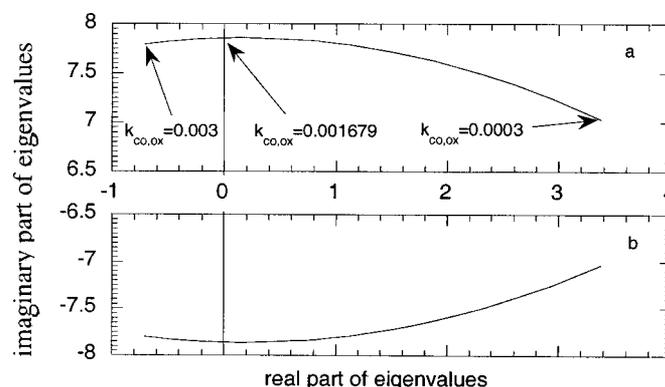

Figure 11. The two complex conjugate eigenvalues of the dynamic model as a function of the CO electro-oxidation rate constant $\vec{k}_{CO,ox}$. This is a complex plain with x-axis being the real part and y-axis the imaginary part of the two complex conjugate eigenvalues.

stability (control method) and possible enhancement in total efficiency under self-sustained oscillation conditions.

List of Symbols

A	geometric area of the electrode in the fuel cell
C_{dl}	anode capacity
C_t^*	atom mole density per cm^2 PtRu surface
F	Faraday constant
i	fuel cell current density
K_C	equilibrium constant for CO desorption (the reciprocal of the adsorption equilibrium constant)
K_H	equilibrium constant for H$_2$ desorption (the reciprocal of the adsorption equilibrium constant)
$\vec{k}_{CO,ad}$	rate constant of CO adsorption
$\vec{k}_{CO,ox}$	rate constant of CO electro-oxidation
$\vec{k}_{H_2,ad}$	rate constant of H$_2$ adsorption
$\vec{k}_{H,ox}$	rate constant of H$_2$ electro-oxidation
$\vec{k}_{OH}$	rate constant of water adsorption
$\overleftarrow{k}_{OH}$	rate constant of water desorption
P_0	standard pressure, 1 atm
p_{H_2}	partial pressure of hydrogen in the anode chamber
R	gas constant
r_{CO}	rate of CO electro-oxidation
$r_{CO,ad}$	net rate of CO adsorption
r_H	rate of H$_2$ electro-oxidation
$r_{H_2,ad}$	net rate of H$_2$ adsorption
r_{OH}	net rate of water dissociation
T	fuel cell temperature
T_0	standard temperature, 298 K
V_A	volume of the anode chamber
v_0	anode inlet volumetric flow rate
v	anode outlet volumetric flow rate
x_{CO}^0	CO mole fraction in the anode feed
x_{CO}	CO mole fraction in the anode chamber

Greek

α_{CO}	transfer coefficient of CO electro-oxidation
α_H	transfer coefficient of hydrogen electro-oxidation
α_{OH}	transfer coefficient of water oxidative dissociation
η_A	anode overpotential
γ	roughness factor of the anode (in the units of cm^2 PtRu/cm^2 electrode)
θ_0	fraction of free surface sites
θ_{CO}	surface coverage of CO
θ_H	surface coverage of H
θ_{OH}	surface coverage of OH

Table A-1. Lumped parameters and base case values in the ODE systems.

A_1	$\dfrac{\vec{k}_{CO,ad}p_{H_2}}{F\gamma C_t^*}$	2.092×10^4 s^{-1}	A_{13}	$\dfrac{A\overleftarrow{k}_{OH}}{C_{dl}}$	3.067×10^4 V s^{-1}
A_2	$\dfrac{\vec{k}_{CO,ad}K_C}{F\gamma C_t^*}$	1.413×10^{-3} s^{-1}	A_{14}	$\dfrac{P_0v_0T}{p_{H_2}V_AT_0}x_{CO}^0$	1.176×10^{-4} s^{-1}
A_3	$\dfrac{1}{F\gamma C_t^*}$	47.11 C^{-1} cm^2	A_{15}	$\dfrac{P_0v_0T}{p_{H_2}V_AT_0}$	1.088 s^{-1}
A_4	$\dfrac{\vec{k}_{H_2,ad}p_{H_2}}{F\gamma C_t^*}$	5.606×10^4 s^{-1}	A_{16}	$\dfrac{ART}{2FV_A}\vec{k}_{H_2,ad}$	1.024×10^3 s^{-1}
A_5	$\dfrac{\vec{k}_{H_2,ad}K_H}{F\gamma C_t^*}$	9.469×10^3 s^{-1}	A_{17}	$\dfrac{ARTK_H}{2Fp_{H_2}V_A}\vec{k}_{H_2,ad}$	1.729×10^2 s^{-1}
A_6	$\dfrac{2\vec{k}_{H,ox}}{F\gamma C_t^*}$	3.769×10^2 s^{-1}	A_{18}	$\dfrac{ART}{FV_A}\vec{k}_{CO,ad}$	7.639×10^2 s^{-1}
A_7	$\dfrac{\vec{k}_{OH}}{F\gamma C_t^*}$	3.769×10^{-2} s^{-1}	A_{19}	$\dfrac{ARTK_C}{Fp_{H_2}V_A}\vec{k}_{CO,ad}$	5.162×10^{-5} s^{-1}
A_8	$\dfrac{\overleftarrow{k}_{OH}}{F\gamma C_t^*}$	1.300×10^5 s^{-1}	α_1	$\dfrac{\alpha_{CO}F}{RT}$	18.42 V^{-1}
A_9	$\dfrac{Ai}{C_{dl}}$	3.333 V s^{-1}	α_2	$\dfrac{\alpha_H F}{RT}$	18.42 V^{-1}
A_{10}	$\dfrac{2A\vec{k}_{H,ox}}{C_{dl}}$	88.89 V s^{-1}	α_3	$\dfrac{\alpha_{OH}F}{RT}$	18.42 V^{-1}
A_{11}	$\dfrac{A}{C_{dl}}$	11.11 F^{-1} cm^2	α_4	$\dfrac{(1-\alpha_{OH})F}{RT}$	18.42 V^{-1}
A_{12}	$\dfrac{A\vec{k}_{OH}}{C_{dl}}$	8.889×10^{-3} V s^{-1}			

Appendix

The system of differential equations is linearized about the stationary state and the stability defined in terms of recovering from a small perturbation. Solving the linearized equations amounts to calculating the eigenvalues of the associated Jacobian matrix. Stability is determined by the sign of these eigenvalues.[7] The mathematical analysis proves that the system experiences a Hopf bifurcation as the electro-oxidation rate constant, $\vec{k}_{CO,ox}$, passes through a critical value.

The ODEs of the model are formulated into a single system in the six dependent variables ($\theta_O, \theta_{CO}, \theta_H, \theta_{OH}, x_{CO}, \eta_A$)

$$\frac{d\theta_{CO}}{dt} = A_1 x_{CO}\theta_0 - A_2\theta_{CO} - A_3\vec{k}_{CO,ox}\theta_{CO}\theta_{OH}\exp(\alpha_1\eta_A) \qquad [A\text{-}1]$$

$$\frac{d\theta_H}{dt} = A_4\theta_0^2 - A_5\theta_H^2 - A_6\theta_H\sinh(\alpha_2\eta_A) \qquad [A\text{-}2]$$

$$\frac{d\theta_{OH}}{dt} = A_7\theta_0\exp(\alpha_3\eta_A) - A_8\theta_{OH}\exp(-\alpha_4\eta_A) - A_3\vec{k}_{CO,ox}\theta_{CO}\theta_{OH}\exp(\alpha_1\eta_A) \qquad [A\text{-}3]$$

$$\frac{d\eta_A}{dt} = A_9 - A_{10}\theta_H\sinh(\alpha_2\eta_A) - A_{11}\vec{k}_{CO,ox}\theta_{CO}\theta_{OH}\exp(\alpha_1\eta_A)$$
$$- A_{12}\theta_0\exp(\alpha_3\eta_A) + A_{13}\theta_{OH}\exp(-\alpha_4\eta_A) \qquad [A\text{-}4]$$

$$\frac{dx_{CO}}{dt} = A_{14} - A_{15}x_{CO} + A_{16}x_{CO}\theta_0^2 - A_{17}x_{CO}\theta_H^2 - A_{18}x_{CO}\theta_0 + A_{19}\theta_{CO} \qquad [A\text{-}5]$$

where A_i and α_i are fixed lumped constants defined in terms of the physical constants but independent of $\vec{k}_{CO,ox}$. The lumped parameters and their corresponding numerical values are listed in Table A-1. In addition to these five equations, the six dependent variables must also satisfy the additional constraint of site balance, namely, $\theta_0 = 1 - \theta_{CO} - \theta_H - \theta_{OH}$.

The equilibrium solution (*i.e.*, a solution that is constant in time) was found numerically for several values of $\vec{k}_{CO,ox}$. Then the Jacobian matrix for the system of differential equations (Eq. A-1 to A-5) was computed and evaluated at the equilibrium points. Finally, the eigenvalues of this matrix were calculated using Maple 7.

The eigenvalues of the system were calculated for various values of the bifurcation parameter $\vec{k}_{CO,ox}$. Three of the five eigenvalues are real and negative as $\vec{k}_{CO,ox}$ varies between 0.0003 and 0.003. The other two are complex conjugate eigenvalues.

References

1. M. L. Perry and T. F. Fuller, *J. Electrochem. Soc.,* **149**, S59 (2002).
2. L. F. Brown, *Int. J. Hydrogen Energy,* **26**, 381 (2001).
3. C. Lamy, A. Lima, V. LeRhun, F. Delime, C. Coutanceau, and J. M. Leger, *J. Power Sources,* **105**, 283 (2002).
4. Z. G. Qi, M. Hollett, A. Attia, and A. Kaufman, *Electrochem. Solid-State Lett.,* **5**, A129 (2002).
5. C. Rice, S. Ha, R. I. Masel, P. Waszczuk, and T. Barnard, *J. Power Sources,* **111**, 83 (2002).
6. K. Krischer, in *Modern Aspects of Electrochemistry,* Vol. 32, J. O'M. Bockris, B. E. Conway, and R. E. White, Editors, p. 1, Plenum, New York (1999).
7. M. T. M. Koper, *J. Chem. Soc., Faraday Trans.,* **94**, 1369 (1998).
8. M. T. M. Koper, T. J. Schmidt, N. M. Markovic, and P. N. Ross, *J. Phys. Chem. B,* **105**, 8381 (2001).
9. J. X. Zhang and R. Datta, *J. Electrochem. Soc.,* **149**, A1423 (2002).
10. J. L. Hudson and T. T. Tsotsis, *Chem. Eng. Sci.,* **49**, 1493 (1994).
11. M. T. M. Koper, *Adv. Chem. Phys.,* **92**, 161 (1996).
12. P. Strasser, *Electrochem. Soc. Interface,* **9**, 46 (2000).
13. P. Strasser, M. Eiswirth, and M. T. M. Koper, *J. Electroanal. Chem.,* **478**, 50 (1999).
14. S. Nakanishi, Y. Mukouyama, and Y. Nakato, *J. Electrochem. Soc.,* **148**, E405 (2001).
15. H. Okamoto, N. Tanaka, and M. Naito, *Chem. Phys. Lett.,* **248**, 289 (1996).
16. W. Wolf, K. Krischer, M. Lubke, M. Eiswirth, and G. Ertl, *J. Electroanal. Chem.,* **385**, 85 (1995).
17. P. Strasser, M. Eiswirth, and G. Ertl, *J. Chem. Phys.,* **107**, 991 (1997).
18. P. Strasser, M. Lubke, P. Parmanada, M. Eiswirth, and G. Ertl, *J. Phys. Chem. B,* **102**, 3227 (1998).
19. J. X. Zhang and R. Datta, *Electrochem. Solid-State Lett.,* **6**, A5 (2003).
20. K. Krischer, M. Lubke, W. Wolf, M. Eiswirth, and G. Ertl, *Ber. Bunsenges. Phys. Chem.,* **95**, 820 (1991).
21. P. Strasser, M. Lubke, F. Raspel, M. Eiswirth, and G. Ertl, *J. Chem. Phys.,* **107**, 979 (1997).
22. T. J. Schmidt, B. N. Grgur, N. M. Markovic, and P. N. Ross, *J. Electroanal. Chem.,* **500**, 36 (2001).
23. C. H. Kim, S. I. Pyun, and H. C. Shin, *J. Electrochem. Soc.,* **149**, A93 (2002).
24. E-TEK catalog, 2002.
25. T. Thampan, S. Malhotra, J. Zhang, and R. Datta, *Catal. Today,* **67**, 15 (2001).

26. K. T. Adjemian, S. J. Lee, S. Srinivasan, J. Benziger, and A. B. Bocarsly, *J. Electrochem. Soc.,* **149**, A256 (2002).
27. H. A. Gasteiger, N. M. Markovic, and P. N. Ross, *J. Phys. Chem.,* **99**, 16757 (1995).
28. N. M. Markovic, C. A. Lucas, B. N. Grgur, and P. N. Ross, *J. Phys. Chem. B,* **103**, 9616 (1999).
29. K. Krischer, M. Lubke, W. Wolf, M. Eiswirth, and G. Ertl, *Electrochim. Acta,* **40**, 69 (1995).
30. W. Wolf, M. Lubke, M. T. M. Koper, K. Krischer, M. Eiswirth, and G. Ertl, *J. Electroanal. Chem.,* **399**, 185 (1995).
31. T. E. Springer, T. Rockward, T. Zawodzinski, and S. Gottesfeld, *J. Electrochem. Soc.,* **148**, A11 (2001).
32. P. Strasser, J. Christoph, W. F. Lin, and M. Eiswirth, *J. Phys. Chem. A,* **104**, 1854 (2000).
33. J. Y. Lee, J. Christoph, P. Strasser, M. Eiswirth, and G. Ertl, *J. Chem. Phys.,* **115**, 1485 (2001).
34. S. C. Cleghorn, C. R. Derouin, M. S. Wilson, and S. Gottesfeld, *J. Appl. Electrochem.,* **28**, 663 (1998).
35. Y. Morimoto, T. Suzuki, and H. Yamada, Abstract 816, The Electrochemical Society Meeting Abstracts, Vol. 2002-2, Salt Lake City, UT, Oct 20-25, 2002.
36. J. Guckenheimer and P. Holmes, *Nonlinear Oscillations, Dynamical Systems, and Bifurcations of Vector Fields*, p. 151, Springer-Verlag, New York (1983).
37. M. C. Deibert and D. L. Williams, *J. Electrochem. Soc.,* **116**, 1291 (1969).